

# Equal-spin and opposite-spin density-density correlations in the BCS-BEC crossover: Gauge Symmetry, Pauli Exclusion Principle, Wick's Theorem and Experiments

Nikolai Kaschewski and Axel Pelster

*Physics Department and Research Center OPTIMAS,  
Rhineland-Palatinate Technical University Kaiserslautern-Landau, 67663 Kaiserslautern, Germany*

Carlos A. R. Sá de Melo

*School of Physics, Georgia Institute of Technology, Atlanta, 30332, USA*

(Dated: February 27, 2026)

We develop a general theory of *spin*-dependent density-density correlations, that is valid for any temperature, interactions, dimensions and mass or population status of Fermi gases with two internal states. We use gauge invariance and the Pauli principle to establish constraints on the *spin*-dependent density-density correlations that are consistent with the fluctuation-dissipation and Wick's theorem. As an example, we study the *spin*-dependent density-density correlations from the BCS to the Bose regime in two dimensions at zero temperature, inspired by experiments in  ${}^6\text{Li}$ . We show that two-particle irreducible contributions involving collective excitations, many-particle scattering and vertex corrections, are essential to describe experiments. In particular they turn out to be responsible for the emergence of an experimentally observed minimum in the opposite-*spin* density-density correlations.

*Introduction:* Ultracold Fermi gases represent a versatile platform to investigate fundamental properties of quantum many-body physics, such as correlations that have been explored in condensed matter [1–5], nuclear physics [6–10], astrophysics [11–14], and ultracold gases [15–22], where the latter serve as quantum simulators [23–26]. The measurement of correlations provide deep insight into degenerate Bose [27–30] and Fermi [31–36] systems. Due to existence of Fano-Feshbach resonances [37–39], a prime example of the manifestation of correlations is the BCS-BEC crossover explored both theoretically [40–45] and experimentally [46–51]. Correlations were further investigated in momentum-frequency space via collective modes in the low-energy-long-wavelength limit [35, 36, 41, 52–58]. However, correlations in real space and time have been little explored because of limited experimental accessibility.

With the recent development of continuous quantum gas microscopes (CQGM) [59–64], it is now possible to directly measure spatially-resolved equal-time density-density correlations in two-dimensional (2D) Fermi gases. These new microscopes differ from previous lattice quantum gas microscopes [24, 26, 65–71] that were restricted to measurements of spatial correlations at large distances only. The CQGM has better spatial resolution than the typical interparticle distance, allowing for the detection of anti-bunching in real space for opposite-*spin* density-density correlations of  ${}^6\text{Li}$  atoms [63] in 2D.

In this letter, we develop a theory of *spin*-dependent density-density correlations, that is valid for any temperature, interactions, dimensions and mass or population status of Fermi gases with two internal states. We derive general constraints that any density-density correlation function in Fermi systems has to fulfill, by making use of the Pauli-principle and gauge symmetry requirements. We find, that those conditions provide us with an equation of state, that is consistent with the fluctuation-

dissipation theorem which then can be separated into two-particle reducible and irreducible terms. To show the power of these constraints we investigate *spin*-dependent density-density correlations from the BCS to the Bose regime in 2D at zero temperature, similar to recent CQGM experiments in  ${}^6\text{Li}$  [63]. We demonstrate that two-particle irreducible contributions arise from taking gauge fixing into account, including collective excitations, many-particle scattering and vertex corrections. It turns out, that incorporating those effects are vital to explain the experiments in the crossover. In particular, we show that irreducible terms are responsible for the emergence of the observed drop of the opposite-*spin* density-density correlation function below the uncorrelated value of one [63]. To make quantitative predictions we ultimately evaluate width and depth of those emerging anti-correlations.

*Correlation functions:* We are interested in the normalized equal-time density-density correlation functions

$$g_{ss'}(\mathbf{r}, \mathbf{r}') = \frac{\langle \hat{n}_s(\mathbf{r}) \hat{n}_{s'}(\mathbf{r}') \rangle}{\langle \hat{n}_s(\mathbf{r}) \rangle \langle \hat{n}_{s'}(\mathbf{r}') \rangle}, \quad (1)$$

where  $\hat{n}_s(\mathbf{r}) = \hat{\psi}_s^\dagger(\mathbf{r}) \hat{\psi}_s(\mathbf{r})$  is the density operator for *spin* projection  $s$ , with  $\hat{\psi}_s^\dagger(\mathbf{r})$  and  $\hat{\psi}_s(\mathbf{r})$  being the field operators for fermions at position  $\mathbf{r}$  in continuum systems. The notation  $\langle \hat{A} \rangle$  denotes the ensemble expectation value of operator  $\hat{A}$  at temperature  $T$ . We use the word *spin* to represent either the internal states of identical fermions with mass  $m_\uparrow = m_\downarrow = m$  or different species of fermions with  $m_\uparrow \neq m_\downarrow$ . For fermions with equal or different masses  $m_\uparrow, m_\downarrow$ , there are two *spin* projections  $s = \{\uparrow, \downarrow\}$ , such that the equal-*spin* (opposite-*spin*) correlation function corresponds to  $s = s'$  ( $s \neq s'$ ).

Before explicitly calculating  $g_{ss'}(\mathbf{r}, \mathbf{r}')$  for a specific Lagrangian, we highlight a few of its symmetries that are independent of dimensionality, interactions, temperature,

masses and population status of *spin* projections.

First, we emphasize the invariance of  $g_{ss'}(\mathbf{r}, \mathbf{r}')$  under the local U(1) gauge transformation  $\hat{\psi}_s(\mathbf{r}) \rightarrow \hat{\psi}_s(\mathbf{r})e^{i\phi_s(\mathbf{r})}$ , since the local density operator  $\hat{n}_s(\mathbf{r})$  is unchanged by it. This is extremely important, because even if the system spontaneously breaks a local U(1) gauge symmetry due to local pairing  $\hat{\psi}_\uparrow(\mathbf{r})\hat{\psi}_\downarrow(\mathbf{r}) \rightarrow \hat{\psi}_\uparrow(\mathbf{r})\hat{\psi}_\downarrow(\mathbf{r})e^{i[\phi_\uparrow(\mathbf{r})+\phi_\downarrow(\mathbf{r})]}$ , the physical  $g_{ss'}(\mathbf{r}, \mathbf{r}')$  must be gauge invariant.

Secondly we investigate the Pauli-principle. Using  $\{\psi_s(\mathbf{r}), \psi_s^\dagger(\mathbf{r}')\} = \delta_{ss'}\delta(\mathbf{r} - \mathbf{r}')$ , we express  $\langle \hat{n}_s(\mathbf{r})\hat{n}_{s'}(\mathbf{r}') \rangle$ , at equal times, in terms of the normal ordered pair correlations  $\langle : \hat{n}_s(\mathbf{r})\hat{n}_{s'}(\mathbf{r}') : \rangle = \langle \psi_s^\dagger(\mathbf{r})\psi_{s'}^\dagger(\mathbf{r}')\psi_{s'}(\mathbf{r}')\psi_s(\mathbf{r}) \rangle$  via the relation  $\langle \hat{n}_s(\mathbf{r})\hat{n}_{s'}(\mathbf{r}') \rangle = \langle : \hat{n}_s(\mathbf{r})\hat{n}_{s'}(\mathbf{r}') : \rangle + \delta_{ss'}\delta(\mathbf{r} - \mathbf{r}')\langle \hat{n}_s(\mathbf{r}) \rangle$ . Using this, we write

$$g_{ss'}(\mathbf{r}, \mathbf{r}') = g_{ss'}^{\text{reg}}(\mathbf{r}, \mathbf{r}') + \frac{\delta_{ss'}\delta(\mathbf{r} - \mathbf{r}')}{\langle \hat{n}_{s'}(\mathbf{r}') \rangle}, \quad (2)$$

where the regular part is

$$g_{ss'}^{\text{reg}}(\mathbf{r}, \mathbf{r}') = \frac{\langle : \hat{n}_s(\mathbf{r})\hat{n}_{s'}(\mathbf{r}') : \rangle}{\langle \hat{n}_s(\mathbf{r}) \rangle \langle \hat{n}_{s'}(\mathbf{r}') \rangle}. \quad (3)$$

We emphasize that the only difference between  $g_{ss'}(\mathbf{r}, \mathbf{r}')$  and  $g_{ss'}^{\text{reg}}(\mathbf{r}, \mathbf{r}')$  in Eqs. (2) and (3) is the singular term that arises for  $s = s'$  and  $\mathbf{r} = \mathbf{r}'$ . The Pauli principle manifests itself in  $\langle : \hat{n}_s(\mathbf{r})\hat{n}_{s'}(\mathbf{r}') : \rangle = 0$  leading to  $\lim_{\mathbf{r} \rightarrow \mathbf{r}'} g_{ss'}^{\text{reg}}(\mathbf{r}, \mathbf{r}') = 0$ , but  $\langle \hat{n}_s(\mathbf{r})\hat{n}_{s'}(\mathbf{r}') \rangle = \delta(\mathbf{0})\langle \hat{n}_s(\mathbf{r}) \rangle$  is singular giving  $\lim_{\mathbf{r} \rightarrow \mathbf{r}'} g_{ss'}(\mathbf{r}, \mathbf{r}') = \delta(\mathbf{0})/\langle \hat{n}_s(\mathbf{r}) \rangle$ .

Using the decomposition  $\hat{n}_s(\mathbf{r}) = \langle \hat{n}_s(\mathbf{r}) \rangle + \delta\hat{n}_s(\mathbf{r})$ , where the ensemble average  $\langle \hat{n}_s(\mathbf{r}) \rangle$  is equal to the local density  $n_s(\mathbf{r})$ , that is,  $\langle \hat{n}_s(\mathbf{r}) \rangle = n_s(\mathbf{r})$ , gives

$$g_{ss'}(\mathbf{r}, \mathbf{r}') = 1 + \frac{\chi_{ss'}(\mathbf{r}, \mathbf{r}')}{n_s(\mathbf{r})n_{s'}(\mathbf{r}')}, \quad (4)$$

where  $\chi_{ss'}(\mathbf{r}, \mathbf{r}') = \langle \delta\hat{n}_s(\mathbf{r})\delta\hat{n}_{s'}(\mathbf{r}') \rangle$  represents the connected density-density correlation tensor. For  $g_{ss'}(\mathbf{r}, \mathbf{r}') = 1$ , the particles at  $\mathbf{r}$  and  $\mathbf{r}'$  are uncorrelated, while for  $g_{ss'}(\mathbf{r}, \mathbf{r}') < 1$ , the fermions exclude each other (correlation holes, anti-bunching) and for  $g_{ss'}(\mathbf{r}, \mathbf{r}') > 1$ , they approach each other (clustering, pairing, bunching). Comparing Eqs. (2) and (4), we write

$$\chi_{ss'}(\mathbf{r}, \mathbf{r}') = \chi_{ss'}^{\text{reg}}(\mathbf{r}, \mathbf{r}') + \delta_{ss'}\delta(\mathbf{r} - \mathbf{r}')n_s(\mathbf{r}), \quad (5)$$

where the regular part of  $\chi_{ss'}(\mathbf{r}, \mathbf{r}')$  is

$$\chi_{ss'}^{\text{reg}}(\mathbf{r}, \mathbf{r}') = \langle : \hat{n}_s(\mathbf{r})\hat{n}_{s'}(\mathbf{r}') : \rangle - n_s(\mathbf{r})n_{s'}(\mathbf{r}'), \quad (6)$$

leading to the manifestation of the Pauli principle as

$$n_s^2(\mathbf{r}) = - \lim_{\mathbf{r} \rightarrow \mathbf{r}'} \chi_{ss}^{\text{reg}}(\mathbf{r}, \mathbf{r}'). \quad (7)$$

The relation in Eq. (7) corresponds to the local equation of state (EoS) that fixes the *spin*-resolved density  $n_s(\mathbf{r})$ . The resulting EoS is consistent with the fluctuation-dissipation theorem [72], that is,

$$\chi_{ss'}(\mathbf{r}, \mathbf{r}') = - \frac{T}{V^2} \frac{\delta^2 \Omega[j_s]}{\delta j_s(\mathbf{r})\delta j_{s'}(\mathbf{r}')}, \quad (8)$$

where  $\Omega[j_s]$  is the thermodynamic potential including the density-fluctuation source terms  $j_s(\mathbf{r})$  and  $j_s(\mathbf{r}')$ . The tensor  $\chi_{ss'}(\mathbf{r}, \mathbf{r}')$  is sometimes called the spatially-dependent compressibility matrix [72].

*Wick's theorem:* Using Wick's decomposition for the equal-time pair correlation function gives

$$\begin{aligned} \langle : \hat{n}_s(\mathbf{r})\hat{n}_{s'}(\mathbf{r}') : \rangle &= \langle \hat{n}_s(\mathbf{r}) \rangle \langle \hat{n}_{s'}(\mathbf{r}') \rangle - |G_{ss'}(\mathbf{r}, \mathbf{r}')|^2 \\ &\quad + |F_{ss'}(\mathbf{r}, \mathbf{r}')|^2 + \langle \hat{n}_s(\mathbf{r})\hat{n}_{s'}(\mathbf{r}') \rangle_{\text{irr}}. \end{aligned} \quad (9)$$

Here, the first term  $\langle \hat{n}_s(\mathbf{r}) \rangle \langle \hat{n}_{s'}(\mathbf{r}') \rangle$  is the product of local densities  $n_s(\mathbf{r})n_{s'}(\mathbf{r}')$ . The second term is the product of the normal (standard) Green's functions  $G_{ss'}(\mathbf{r}, \mathbf{r}') = \langle \hat{\psi}_s^\dagger(\mathbf{r})\hat{\psi}_{s'}(\mathbf{r}') \rangle$ . The third term is the product of anomalous (pair) Green's functions  $F_{ss'}(\mathbf{r}, \mathbf{r}') = \langle \hat{\psi}_s(\mathbf{r})\hat{\psi}_{s'}(\mathbf{r}') \rangle$ . The last term  $\langle \hat{n}_s(\mathbf{r})\hat{n}_{s'}(\mathbf{r}') \rangle_{\text{irr}} = \langle \delta\hat{n}_s(\mathbf{r})\delta\hat{n}_{s'}(\mathbf{r}') \rangle_{\text{irr}}$  is the two-particle irreducible part of the *spin*-dependent density-density correlations.

Using Wick's theorem in Eq. (9) and the relation in Eq. (6), we write

$$\chi_{ss'}^{\text{reg}}(\mathbf{r}, \mathbf{r}') = \chi_{\text{red},ss'}(\mathbf{r}, \mathbf{r}') + \chi_{\text{irr},ss'}(\mathbf{r}, \mathbf{r}'), \quad (10)$$

where the two-particle reducible contribution is

$$\chi_{\text{red},ss'}(\mathbf{r}, \mathbf{r}') = -|G_{ss'}(\mathbf{r}, \mathbf{r}')|^2 + |F_{ss'}(\mathbf{r}, \mathbf{r}')|^2, \quad (11)$$

while the two-particle irreducible contribution reads

$$\chi_{\text{irr},ss'}(\mathbf{r}, \mathbf{r}') = \langle \delta\hat{n}_s(\mathbf{r})\delta\hat{n}_{s'}(\mathbf{r}') \rangle_{\text{irr}}. \quad (12)$$

Combining Eqs. (2) and (10), we write

$$g_{ss'}^{\text{reg}}(\mathbf{r}, \mathbf{r}') = 1 + \delta g_{\text{red},ss'}(\mathbf{r}, \mathbf{r}') + \delta g_{\text{irr},ss'}(\mathbf{r}, \mathbf{r}'), \quad (13)$$

where the contributions from correlations are  $\delta g_{\alpha,ss'}(\mathbf{r}, \mathbf{r}') = \chi_{\alpha,ss'}(\mathbf{r}, \mathbf{r}')/n_s(\mathbf{r})n_{s'}(\mathbf{r}')$ , with  $\alpha \in \{\text{red}, \text{irr}\}$ , corresponding to deviations from one, that is the uncorrelated limit. Furthermore, the Pauli principle from Eq. (7), separates the local EoS into reducible and irreducible contributions

$$n_s^2(\mathbf{r}) = - \lim_{\mathbf{r} \rightarrow \mathbf{r}'} [\chi_{\text{red},ss}(\mathbf{r}, \mathbf{r}') + \chi_{\text{irr},ss}(\mathbf{r}, \mathbf{r}')]. \quad (14)$$

For translationally invariant systems  $n_s(\mathbf{r}) = n_s$ , the general relations from Eqs. (13) and (14) become

$$n_s^2 = - \lim_{\delta\mathbf{r} \rightarrow \mathbf{0}} [\chi_{\text{red},ss}(\delta\mathbf{r}) + \chi_{\text{irr},ss}(\delta\mathbf{r})], \quad (15)$$

for the EoS that obeys the Pauli principle, and

$$g_{ss'}^{\text{reg}}(\delta\mathbf{r}) = 1 + \delta g_{\text{red},ss'}(\delta\mathbf{r}) + \delta g_{\text{irr},ss'}(\delta\mathbf{r}), \quad (16)$$

for the normalized *spin*-resolved density-density correlation function. Here,  $\delta\mathbf{r} = \mathbf{r}' - \mathbf{r}$  is the relative position and  $\delta g_{\alpha,ss'}(\delta\mathbf{r}) = \chi_{\alpha,ss'}(\delta\mathbf{r})/n_s n_{s'}$  are the contributions from correlations.

Next, we discuss a translationally invariant continuum model for the BCS-BEC crossover, obtaining explicitly the *spin*-resolved density-density response and the EoS.

*BCS-BEC crossover:* We consider a *spin* mixture of fermions in  $D$ -dimensions with *spin*  $s = \{\uparrow, \downarrow\}$  described by the Lagrangian density

$$\mathcal{L} = \sum_s \bar{\psi}_s(x) \left[ \partial_\tau - \frac{\nabla^2}{2m_s} - \mu_s \right] \psi_s(x) \quad (17)$$

$$- g \bar{\psi}_\uparrow(x) \bar{\psi}_\downarrow(x) \psi_\downarrow(x) \psi_\uparrow(x) - \sum_s j_s(x) n_s(x)$$

defined in the volume  $L^D$ . Here,  $\bar{\psi}_s(x)$  and  $\psi_s(x)$ , having dimensions  $L^{-D/2}$ , are the Grassmann fields of *spin*  $s$  describing field operators  $\hat{\psi}_s^\dagger(x)$  and  $\hat{\psi}_s(x)$  at  $x = (\mathbf{r}, \tau)$ , where  $\mathbf{r}$  is the position and  $\tau \in [0, \beta]$  is the imaginary time. Furthermore,  $\mu_s$  is the chemical potential,  $m_s$  the mass of the *spin* species and  $g \geq 0$  is the local SU(2)-invariant attractive interaction strength with dimensions of energy times volume. We use  $\beta = 1/T$  as inverse temperature and units where  $k_B = 1 = \hbar$ .

The Lagrangian density  $\mathcal{L}$  includes a coupling between real *spin*-dependent source fields  $j_s(x)$  with dimensions of energy, and real density fields  $n_s(x)$  with dimensions of inverse volume, leading to the dimensionless action  $\mathcal{S}[\bar{\psi}, \psi; j_s] = \int dx \mathcal{L}$  with  $\int dx = \int_0^\beta d\tau \int_{L^D} d^D r$  used to obtain the source-dependent thermodynamic potential  $\Omega[j_s] = -T \ln \mathcal{Z}[j_s]$ , where the source-dependent partition function is  $\mathcal{Z}[j_s] = \oint \mathcal{D}[\bar{\psi}, \psi] e^{-\mathcal{S}[\bar{\psi}, \psi; j_s]}$ .

To compute the *spin*-resolved density-density correlator in the superfluid state, we decouple the interaction in terms of the complex pair field  $\Delta(x)$  via a Hubbard-Stratonovich transformation [73, 74], and go to Fourier space. Integrating out the fermions and the pair fluctuations, see End Matter, leads to the action contribution

$$\mathcal{S}_2[j_s] = \frac{\beta}{2} \sum_q \mathbf{j}_q^T \tilde{\chi}(q) \mathbf{j}_q, \quad (18)$$

where the *spin*-resolved density-density tensor, with dimensions of inverse energy, is

$$\tilde{\chi}(q) = \tilde{\chi}_0(q) + \tilde{\chi}_{\text{irr}}(q). \quad (19)$$

Here,  $\mathbf{j}_q^T$  is the Fourier transform of  $\mathbf{j}^T(x) = (j_\uparrow(x), j_\downarrow(x))$ , and  $q = (\mathbf{q}, iq_\ell)$ , where  $\mathbf{q}$  is the momentum and  $q_\ell$  is the bosonic Matsubara frequency. In Eq. (19),  $\tilde{\chi}(q)$  is an approximate, Pauli-principle preserving and gauge-invariant solution to the generalized Bethe-Salpeter equation [75], with elements  $\tilde{\chi}_{ss'}(q) = L^D \int_0^\beta d\delta\tau \int d^D \delta\mathbf{r} \chi_{ss'}(\delta\mathbf{r}, \delta\tau) e^{-i\mathbf{q}\delta\mathbf{r} + iq_\ell \delta\tau}$ , using  $\chi_{ss'}(\delta\mathbf{r}, \delta\tau) = \langle \delta\hat{n}_s(\mathbf{0}, 0) \delta\hat{n}_{s'}(\delta\mathbf{r}, \delta\tau) \rangle$ .

The matrix  $\tilde{\chi}_0(q)$  describes the connected reducible *spin*-resolved density-density response including both  $\chi_{\text{red}, ss'}(\delta\mathbf{r})$  from Eq. (11) and a constant term arising from the singular part of  $\chi_{ss'}(\delta\mathbf{r})$ , defined in Eq. (5), when  $n_s(\mathbf{r}) = n_s$ . The second term  $\tilde{\chi}_{\text{irr}}(q)$  represents the two-particle irreducible contribution describing collective excitations, many-body scattering states and vertex corrections, as discussed in Eq. (12) for its real-space counterpart.

Case	Approximation	Gauge	Pauli	Line style
I	SP EoS + only $\chi_{ss'}^{(0)}$	✓	✓	dashed black
II	SP EoS + full $\chi_{ss'}$	✓	×	dotted green
III	GF EoS + full $\chi_{ss'}$	✓	×	dash-dotted red
IV	PR EoS + full $\chi_{ss'}$	✓	✓	solid blue

TABLE I. Table for different cases covering distinct levels of approximation, depending on the preservation (✓) or violation (×) of gauge invariance (Gauge) and the Pauli principle (Pauli) of the approximation used to compute the correlation function  $\chi_{ss'}$ . Gauge invariance applied to EoS ( $\chi_{ss'}$ ) is global (local). The corresponding line styles used in the subsequent figures are also indicated.

To obtain the Gaussian fluctuation (GF) EoS, arising only from pair fluctuations, we set  $j_s = 0$  and use  $\Omega = -T \ln \mathcal{Z}[j_s = 0]$  to give  $n_s = n_{s, \text{sp}} + n_{s, \text{fl}}$ . Here, the first term  $n_{s, \text{sp}}$  comes from the saddle-point and the second  $n_{s, \text{fl}}$  is due to pair fluctuations, see Eq. (A15) in the End Matter. The GF EoS is globally gauge-invariant, in the sense that it depends only on the order-parameter modulus  $|\Delta_0|$ , but violates the Pauli principle, because it does not include the irreducible two-particle contributions.

Making the identifications  $\lim_{\delta\mathbf{r} \rightarrow \mathbf{0}} \chi_{\text{red}, ss'}(\delta\mathbf{r}) = \sum_q \tilde{\chi}_{\text{red}, ss'}(q) / (\beta L^{2D})$  for the reducible part and  $\lim_{\delta\mathbf{r} \rightarrow \mathbf{0}} \chi_{\text{irr}, ss'}(\delta\mathbf{r}) = \sum_q \tilde{\chi}_{\text{irr}, ss'}(q) / (\beta L^{2D})$ , for the irreducible component, Eq. (15) becomes

$$n_s^2 = -\frac{1}{\beta L^{2D}} \sum_q \tilde{\chi}_{\text{red}, ss}(q) - \frac{1}{\beta L^{2D}} \sum_q \tilde{\chi}_{\text{irr}, ss}(q), \quad (20)$$

representing the Pauli-respecting (PR) EoS, which is also gauge invariant. The solutions of the different EoS are discussed in Fig. 4 in the End Matter.

Next, we investigate  $\chi_{ss'}(\delta\mathbf{r}) = \langle \delta\hat{n}_s(\mathbf{0}) \delta\hat{n}_{s'}(\delta\mathbf{r}) \rangle$  and  $g_{ss'}(\delta\mathbf{r})$  for the BCS-BEC crossover in two dimensions particularized to  $T = 0$ , equal masses and populations to compare with recent experiments [63] close to this limiting case.

*Correlation functions in 2D:* Particularizing to  $T = 0$  and using rotational invariance, we obtain

$$\chi_{ss'}(|\delta\mathbf{r}|) = \frac{1}{L^2} \int_{-\infty}^{\infty} \frac{dq_\ell}{2\pi} \int_0^{\infty} \frac{dQ}{2\pi} Q \tilde{\chi}_{ss'}(Q, iq_\ell) J_0(Q|\delta\mathbf{r}|), \quad (21)$$

where integration over the azimuthal angle leads to the zeroth order Bessel function  $J_0(Q|\delta\mathbf{r}|)$  with  $|\delta\mathbf{r}|$  and  $Q = |\mathbf{q}|$  being the modulus of  $\delta\mathbf{r}$  and  $\mathbf{q}$ , respectively.

We apply the Lippmann-Schwinger relation [76] to replace the interaction  $g$  by the two-body bound state energy  $\varepsilon_B > 0$ , and use the Fermi momentum (energy)  $k_F$  ( $\varepsilon_F$ ) to relate  $\varepsilon_B$  to the 2D scattering length  $a$  as  $\ln k_F a = \ln(8\varepsilon_F/\varepsilon_B)/2 - \gamma_E$ , with  $\gamma_E$  as Euler constant.

In Fig. 1, we illustrate the behavior of  $g_{ss'}(\delta\mathbf{r})$ , defined in Eq. (16), and of the full density-density correlation function  $g_{nn}(\delta\mathbf{r}) = \sum_{ss'} g_{ss'}(\delta\mathbf{r})$  versus separation  $k_F |\delta\mathbf{r}|$ . The interaction parameters are  $\ln k_F a = 2.15$

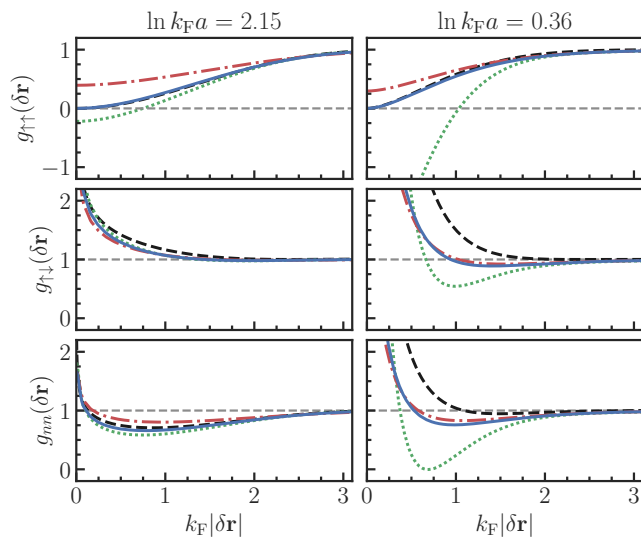


FIG. 1. Plots of spatial behavior of the correlation functions  $g_{ss'}(\delta\mathbf{r})$  and of  $g_{nn}(\delta\mathbf{r})$  for translationally and rotationally invariant systems. The interaction parameters are  $\ln k_F a = 2.15$  (BCS regime) and  $\ln k_F a = 0.36$  (crossover region). The line types indicate the level of approximation used, see Table I.

(BCS regime) and  $\ln k_F a = 0.36$  (crossover region). The different level of approximations and line types are summarized in Table I. For  $g_{\uparrow\uparrow}(\delta\mathbf{r})$ , the dotted green lines (case II) and dash-dotted red lines (case III) violate the Pauli exclusion principle, while the dashed black lines (case I) and the solid blue lines (case IV) satisfy it. For  $g_{\uparrow\downarrow}(\delta\mathbf{r})$  the dotted green lines (case II) dash-dotted red lines (case III) do not differ substantially from the dashed black lines (case I) and the solid blue lines (case IV) in the BCS regime ( $\ln k_F a = 2.15$ ), but start to behave differently in the crossover region ( $\ln k_F a = 0.36$ ) and beyond, due to contributions from the two-particle irreducible terms. The main purpose of Fig. 1 is to show that the approximations used in cases II and III of Table I are gauge invariant but violate the Pauli principle, while the approaches in cases I and IV satisfy both gauge invariance and the Pauli principle.

In Fig. 2, we show only cases I and IV, where we plot the correlation functions  $g_{\uparrow\uparrow}(|\delta\mathbf{r}|)$ ,  $g_{\uparrow\downarrow}(|\delta\mathbf{r}|)$ ,  $g_{nn}(|\delta\mathbf{r}|)$  versus  $k_F|\delta\mathbf{r}|$  for the set of parameters  $\ln k_F a = \{2.15, 1.01, 0.36\}$ , used in experiments [62]. An extended version of Fig. 2 is found in Fig. 5 in the End Matter.

In Fig. 2 (top panel), we illustrate that the difference between cases I and IV is small for  $g_{\uparrow\uparrow}(\delta\mathbf{r})$  for the parameters shown. In case I, the only contributions to  $g_{\uparrow\uparrow}(\delta\mathbf{r})$  in Eq. (13) are from the two-particle reducible correlations  $\delta g_{\text{red},\uparrow\uparrow}(\delta\mathbf{r}) = \chi_{\text{red},\uparrow\uparrow}(\delta\mathbf{r})/n_{\uparrow}^2 = -|G_{\uparrow\uparrow}(\delta\mathbf{r})|^2/n_{\uparrow}^2$ . This is due to the absence of triplet pairing in our model, that is  $F_{\uparrow\uparrow}(\delta\mathbf{r}) = 0$ . This term is comparable to the sum of  $\delta g_{\text{red},\uparrow\uparrow}(\delta\mathbf{r})$  and  $\delta g_{\text{irr},\uparrow\uparrow}(\delta\mathbf{r}) = \chi_{\text{irr},\uparrow\uparrow}(\delta\mathbf{r})/n_{\uparrow}^2$  in case IV, due to the absence of triplet pairing in our model. The half-width  $k_{Fp}$  describes the size of *Pauli hole* in  $g_{\uparrow\uparrow}(\delta\mathbf{r})$ .

In Fig. 2 (middle panel), we show that differences be-

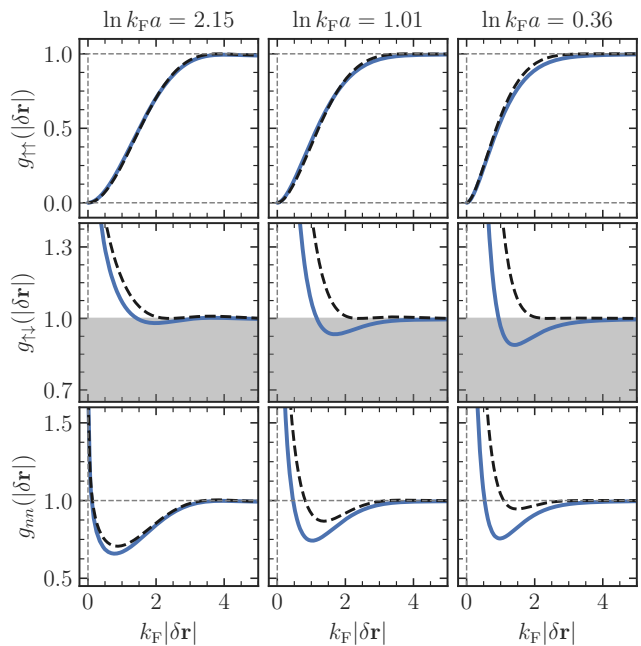


FIG. 2. Numerical results for  $g_{\uparrow\uparrow}(\delta\mathbf{r})$  ranging from 0 and 1 (top panel),  $g_{\uparrow\downarrow}(\delta\mathbf{r})$  (middle panel) ranging from 0.7 to 1.4 and  $g_{nn}(\delta\mathbf{r})$  (bottom panel) ranging from 0.5 to 1.5 versus distance  $k_F|\delta\mathbf{r}|$  ranging from 0 to 5. The dashed black (solid blue) lines illustrate case I (IV) in Table I. The gray region in the middle panel shows that  $g_{\uparrow\downarrow}(\delta\mathbf{r}) \geq 1$  with no minimum for the dashed black line, while  $g_{\uparrow\downarrow}(\delta\mathbf{r})$  has a clear minimum below 1 for the solid blue line. The interaction parameter  $\ln k_F a$  ranges from 2.15 (BCS regime) to 0.36 (crossover region) and are closely related to the experimental values [63].

tween cases I and IV are more dramatic for  $g_{\uparrow\downarrow}(\delta\mathbf{r})$  for the parameters shown. In case I, the only contribution to  $g_{\uparrow\downarrow}(\delta\mathbf{r})$  in Eq. (13) is from the two-particle reducible correlations  $\delta g_{\text{red},\uparrow\downarrow} = \chi_{\text{red},\uparrow\downarrow}(\delta\mathbf{r})/n_{\uparrow}n_{\downarrow} = |F_{\uparrow\downarrow}(\delta\mathbf{r})|^2/n_{\uparrow}n_{\downarrow}$  which is always positive (bunching). There is no negative contribution arising, since  $G_{\uparrow\downarrow}(\delta\mathbf{r}) = 0$  due to the SU(2)-symmetry of the contact interaction. However, in case IV, there are two contributions:  $\delta g_{\text{red},\uparrow\downarrow}(\delta\mathbf{r})$ , which is always positive, and  $\delta g_{\text{irr},\uparrow\downarrow}(\delta\mathbf{r})$  which is always negative (anti-bunching) due to the coupling to pair fluctuations. Case I (dashed black line) always gives  $g_{\uparrow\downarrow}(\delta\mathbf{r}) \geq 1$  and does not produce a minimum in  $g_{\uparrow\downarrow}(\delta\mathbf{r})$ . The minimum in  $g_{\uparrow\downarrow}(\delta\mathbf{r})$  arises from the interplay between two-particle reducible and irreducible contributions, where the latter are included only in case IV (solid blue line).

In Fig. 2 (bottom panel), we show that cases I and IV also differ substantially for  $g_{nn}(\delta\mathbf{r})$ , for the parameters used, due to the differences in  $g_{\uparrow\downarrow}(\delta\mathbf{r})$ . Both cases I and IV produce a minimum for  $g_{nn}(\delta\mathbf{r})$  due to the increase in  $g_{\uparrow\uparrow}(\delta\mathbf{r}) = g_{\downarrow\downarrow}(\delta\mathbf{r})$  and the decrease in  $g_{\uparrow\downarrow}(\delta\mathbf{r}) = g_{\downarrow\uparrow}(\delta\mathbf{r})$  with growing  $k_F|\delta\mathbf{r}|$  from 0 to  $\lesssim 1$ , in the range of parameters shown. However, the location and depth of the minimum in  $g_{nn}(\delta\mathbf{r})$  is different from that of  $g_{\uparrow\downarrow}(\delta\mathbf{r})$ . To clarify this behavior further, we discuss next the location

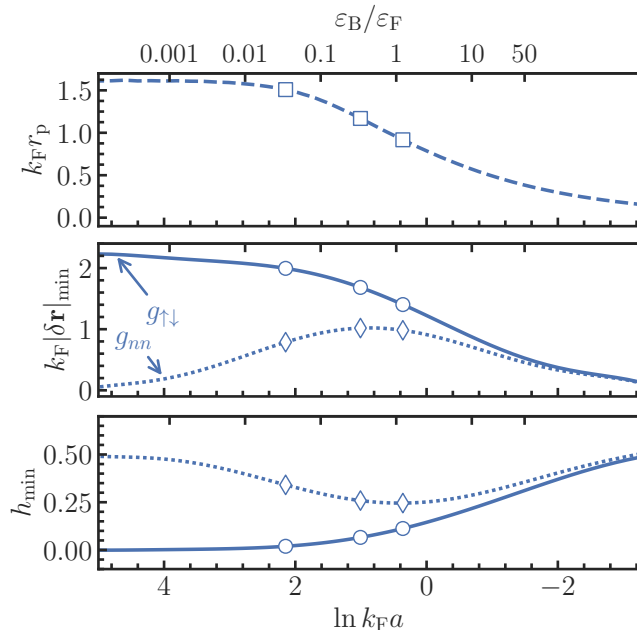


FIG. 3. Plots of  $k_{Fp}$  (top panel),  $k_F|\delta\mathbf{r}|_{\min}$  (middle panel),  $h_{\min}$  (bottom panel), versus  $\ln k_F a$ . The depth of the minimum is  $h_{\min} = |g_{\uparrow\downarrow}(\delta\mathbf{r}_{\min}) - 1|$  or  $h_{\min} = |g_{nn}(\delta\mathbf{r}_{\min}) - 1|$ . The solid blue lines refer to  $g_{\uparrow\downarrow}(\delta\mathbf{r})$ , the dotted blue lines represent  $g_{\uparrow\downarrow}(\delta\mathbf{r})$ , and the dashed blue line reflects  $g_{\uparrow\uparrow}(\delta\mathbf{r})$ . The blue circles, diamonds and squares describe the scattering parameters used in Fig. 2.

and depth of the minima in  $g_{\uparrow\downarrow}(\delta\mathbf{r})$  and  $g_{nn}(\delta\mathbf{r})$ , as well as the half-width of the *Pauli hole*,  $k_{Fp}$ , in  $g_{\uparrow\uparrow}(\delta\mathbf{r})$ .

In Fig. 3, we show  $k_{Fp}$  (top panel), the position of the minimum  $k_F|\delta\mathbf{r}|_{\min}$  (middle panel) in  $g_{\uparrow\downarrow}(\delta\mathbf{r})$  and  $g_{nn}(\delta\mathbf{r})$ , as well as, its depth  $h_{\min}$  (bottom panel) versus  $\ln k_F a$ , for case IV only. As seen in the top panel,  $k_{Fp}$  becomes smaller with increasing  $\ln k_F a$  approaching zero asymptotically in the extreme Bose regime for low densities. The location and depth of the minimum in  $g_{\uparrow\downarrow}(\delta\mathbf{r})$  and  $g_{nn}(\delta\mathbf{r})$  differ substantially in the BCS regime, because  $k_{Fp}$  is sufficiently large to produce a

deeper minimum and shorter distances in  $g_{nn}(\delta\mathbf{r})$ . However, as  $k_{Fp}$  shrinks with increasing  $\ln k_F a$ , the location  $k_F|\delta\mathbf{r}|_{\min}$  and depth  $h_{\min}$  of  $g_{nn}(\delta\mathbf{r})$  approaches those of  $g_{\uparrow\downarrow}(\delta\mathbf{r})$ , since those correlations grow more important.

*Conclusions:* In this letter we established fundamental constraints for *spin*-dependent density-density correlations, irrespective of temperature, interactions, dimensionality and mass or population status of Fermi *spin*-mixtures. Those arise from fundamental requirements only, that are the Pauli-principle and the necessity of gauge invariance of density-density correlations. After this we presented a physical interpretation for the arising constraints by comparing with Wick's theorem. As an example, we then investigated the *spin*-dependent density-density correlations of a Fermi *spin*-mixture in 2D and at  $T = 0$ . In particular we focused on interaction strengths accessible in recent  ${}^6\text{Li}$  experiments [63]. With this we demonstrated, that two-particle irreducible contributions are responsible for the differences between saddle-point and fluctuation approaches. Those irreducible terms slow down the reduction of *Pauli hole*'s width with increasing interactions in comparison to saddle-point results; they are responsible for the emergence of a minimum in the opposite-*spin* density-density correlations, which is absent in saddle-point theories, in agreement with recent experimental investigations [63].

As an outlook, we will perform calculations at finite temperatures, which are technically more challenging, because it is necessary to handle branch cuts and poles (collective excitations) of the correlation function with the additional complication of including vortices and antivortices in two-dimensions.

*Note added:* During the writing of our work, we became aware of a very recent pre-print [77], that also addresses experiments [63] using a different approach.

*Acknowledgments:* We thank Joshua Krauss, Flavia Braga Ramos and Sejung Yong for discussions. C. A. R. SdM thanks the German Research Foundation (Mercator Fellowship) for support. We acknowledge financial support by the Deutsche Forschungsgemeinschaft (DFG, German Research Foundation) via the Collaborative Research Center SFB/TR185 (Project No. 277625399).

- 
- [1] T. Kaneko, H. Sakakibara, M. Ochi, and K. Kuroki, Pair correlations in the two-orbital Hubbard ladder: Implications for superconductivity in the bilayer nickelate  $\text{La}_3\text{Ni}_2\text{O}_7$ , *Phys. Rev. B* **109**, 045154 (2024).
  - [2] C.-H. Huang, A. Skurativska, F. S. Bergeret, and M. A. Cazalilla, Probing magnetic and triplet correlations in spin-split superconductors with magnetic impurities, *Phys. Rev. Res.* **6**, 033022 (2024).
  - [3] J. C. Estrada Saldaña, A. Vekris, L. Pavešič, R. Žitko, K. Grove-Rasmussen, and J. Nygård, Correlation between two distant quasiparticles in separate superconducting islands mediated by a single spin, *Nat. Commun.* **15**, 3465 (2024).
  - [4] M. Thumin and G. Bouzerar, Correlation functions and characteristic length scales in flat band superconductors, *SciPost Phys.* **18**, 025 (2025).
  - [5] D. K. Mark, H.-Y. Hu, J. Kwan, C. Kokail, S. Choi, and S. F. Yelin, Efficiently Measuring *d*-Wave Pairing and Beyond in Quantum Gas Microscopes, *Phys. Rev. Lett.* **135**, 123402 (2025).
  - [6] A. A. Isayev, Correlation functions for a di-neutron condensate in asymmetric nuclear matter, *Phys. Rev. C* **78**, 014306 (2008).
  - [7] N. Pillet, N. Sandulescu, P. Schuck, and J.-F. Berger, Two-particle spatial correlations in superfluid nuclei, *Phys. Rev. C* **81**, 034307 (2010).
  - [8] E. B. Balbutsev, L. A. Malov, and P. Schuck, Spatial dependence of pairing in deformed nuclei, *Phys. At. Nucl.*

- 74**, 1651 (2011).
- [9] R.-D. Lasserri, J.-P. Ebran, E. Khan, and N. Sandulescu, Localization of pairing correlations in nuclei within relativistic mean field models, *Phys. Rev. C* **98**, 014310 (2018).
- [10] E. Litvinova and P. Schuck, Many-body correlations in nuclear superfluidity, *Phys. Rev. C* **102**, 034310 (2020).
- [11] T. Frick, H. Mütter, A. Rios, A. Polls, and A. Ramos, Correlations in hot asymmetric nuclear matter, *Phys. Rev. C* **71**, 014313 (2005).
- [12] H.-F. Zhu, X. Wu, and G.-Z. Liu, Nonperturbative study of quantum many-body correlation effects in neutron stars: Equation of state, *Phys. Rev. C* **110**, 035810 (2024).
- [13] A. Sedrakian, Short-Range Correlations and Urca Process in Neutron Stars, *Phys. Rev. Lett.* **133**, 171401 (2024).
- [14] N. Chamel, Superfluid fraction in the crystalline crust of a neutron star: Role of BCS pairing, *Phys. Rev. C* **111**, 045803 (2025).
- [15] G. B. Partridge, K. E. Strecker, R. I. Kamar, M. W. Jack, and R. G. Hulet, Molecular Probe of Pairing in the BEC-BCS Crossover, *Phys. Rev. Lett.* **95**, 020404 (2005).
- [16] G. E. Astrakharchik, J. Boronat, J. Casulleras, and S. Giorgini, Equation of State of a Fermi Gas in the BEC-BCS Crossover: A Quantum Monte Carlo Study, *Phys. Rev. Lett.* **93**, 200404 (2004).
- [17] C. Lobo, I. Carusotto, S. Giorgini, A. Recati, and S. Stringari, Pair Correlations of an Expanding Superfluid Fermi Gas, *Phys. Rev. Lett.* **97**, 100405 (2006).
- [18] S. Gandolfi, K. E. Schmidt, and J. Carlson, BEC-BCS crossover and universal relations in unitary Fermi gases, *Phys. Rev. A* **83**, 041601 (2011).
- [19] F. Werner and Y. Castin, General relations for quantum gases in two and three dimensions: Two-component fermions, *Phys. Rev. A* **86**, 013626 (2012).
- [20] L. He, Dynamic density and spin responses of a superfluid Fermi gas in the BCS–BEC crossover: Path integral formulation and pair fluctuation theory, *Ann. Phys. (New York)* **373**, 470 (2016).
- [21] J. C. Obeso-Jureidini and V. Romero-Rochín, Density correlation functions and the spatial structure of the two-dimensional BEC-BCS crossover, *Phys. Rev. A* **105**, 043307 (2022).
- [22] J. C. Obeso-Jureidini, G. A. Domínguez-Castro, E. Neri, R. Paredes, and V. Romero-Rochín, Universal correlations along the BEC-BCS crossover, *New J. Phys.* **25**, 113019 (2023).
- [23] I. Bloch, J. Dalibard, and S. Nascimbène, Quantum simulations with ultracold quantum gases, *Nat. Phys.* **8**, 267 (2012).
- [24] C. Gross and I. Bloch, Quantum simulations with ultracold atoms in optical lattices, *Science* **357**, 995 (2017).
- [25] P. van Wyk, H. Tajima, D. Inotani, A. Ohnishi, and Y. Ohashi, Superfluid Fermi atomic gas as a quantum simulator for the study of the neutron-star equation of state in the low-density region, *Phys. Rev. A* **97**, 013601 (2018).
- [26] A. J. Daley, I. Bloch, C. Kokail, S. Flannigan, N. Pearson, M. Troyer, and P. Zoller, Practical quantum advantage in quantum simulation, *Nature* **607**, 667 (2022).
- [27] T. M. Wright, A. Perrin, A. Bray, J. Schmiedmayer, and K. V. Kheruntsyan, Two-body anticorrelation in a harmonically trapped ideal bose gas, *Phys. Rev. A* **86**, 023618 (2012).
- [28] T. Schweigler, V. Kasper, S. Erne, I. Mazets, B. Rauer, F. Cataldini, T. Langen, T. Gasenzer, J. Berges, and J. Schmiedmayer, Experimental characterization of a quantum many-body system via higher-order correlations, *Nature* **545**, 323 (2017).
- [29] T. V. Zache, T. Schweigler, S. Erne, J. Schmiedmayer, and J. Berges, Extracting the Field Theory Description of a Quantum Many-Body System from Experimental Data, *Phys. Rev. X* **10**, 011020 (2020).
- [30] T. Schweigler, M. Gluza, Marekand Tajik, S. Sotiriadis, F. Cataldini, S.-C. Ji, F. S. Møller, J. Sabino, B. Rauer, J. Eisert, and J. Schmiedmayer, Decay and recurrence of non-Gaussian correlations in a quantum many-body system, *Nat. Phys.* **17**, 559 (2021).
- [31] M. Greiner, C. A. Regal, J. T. Stewart, and D. S. Jin, Probing Pair-Correlated Fermionic Atoms through Correlations in Atom Shot Noise, *Phys. Rev. Lett.* **94**, 110401 (2005).
- [32] S. Fölling, F. Gerbier, A. Widera, O. Mandel, T. Gericke, and I. Bloch, Spatial quantum noise interferometry in expanding ultracold atom clouds, *Nature* **434**, 481 (2005).
- [33] A. Schirotzek, Y.-i. Shin, C. H. Schunck, and W. Ketterle, Determination of the Superfluid Gap in Atomic Fermi Gases by Quasiparticle Spectroscopy, *Phys. Rev. Lett.* **101**, 140403 (2008).
- [34] K. Hueck, N. Luick, L. Sobirey, J. Siegl, T. Lompe, and H. Moritz, Two-Dimensional Homogeneous Fermi Gases, *Phys. Rev. Lett.* **120**, 060402 (2018).
- [35] H. Biss, L. Sobirey, N. Luick, M. Bohlen, J. J. Kinnunen, G. M. Bruun, T. Lompe, and H. Moritz, Excitation Spectrum and Superfluid Gap of an Ultracold Fermi Gas, *Phys. Rev. Lett.* **128**, 100401 (2022).
- [36] X. Li, S. Wang, X. Luo, Y.-Y. Zhou, K. Xie, H.-C. Shen, Y.-Z. Nie, Q. Chen, H. Hu, Y.-A. Chen, X.-C. Yao, and J.-W. Pan, Observation and quantification of the pseudogap in unitary Fermi gases, *Nature* **626**, 288 (2024).
- [37] H. Feshbach, Unified theory of nuclear reactions, *Ann. Phys. (New York)* **5**, 357 (1958).
- [38] U. Fano, Effects of Configuration Interaction on Intensities and Phase Shifts, *Phys. Rev.* **124**, 1866 (1961).
- [39] C. Chin, R. Grimm, P. Julienne, and E. Tiesinga, Feshbach resonances in ultracold gases, *Rev. Mod. Phys.* **82**, 1225 (2010).
- [40] C. A. R. Sá de Melo, M. Randeria, and J. R. Engelbrecht, Crossover from BCS to Bose superconductivity: Transition temperature and time-dependent Ginzburg-Landau theory, *Phys. Rev. Lett.* **71**, 3202 (1993).
- [41] J. R. Engelbrecht, M. Randeria, and C. A. R. Sá de Melo, BCS to Bose crossover: Broken-symmetry state, *Phys. Rev. B* **55**, 15153 (1997).
- [42] A. Perali, P. Pieri, L. Pisani, and G. C. Strinati, BCS-BEC Crossover at Finite Temperature for Superfluid Trapped Fermi Atoms, *Phys. Rev. Lett.* **92**, 220404 (2004).
- [43] J. Hofmann and W. Zwerger, Deep inelastic scattering on ultracold gases, *Phys. Rev. X* **7**, 011022 (2017).
- [44] H. Deng, C. Li, Y. Wu, L. Sun, and Q. Chen, Flat band effects on the ground-state BCS-BEC crossover in atomic Fermi gases in a quasi-two-dimensional Lieb lattice, *Annals of Physics* **463**, 169639 (2024).
- [45] E. Dizer, J. Horak, and J. M. Pawłowski, Spectral properties and observables in ultracold Fermi gases, *Phys. Rev. A* **109**, 063311 (2024).

- [46] B. Mukherjee, P. B. Patel, Z. Yan, R. J. Fletcher, J. Struck, and M. W. Zwierlein, Spectral Response and Contact of the Unitary Fermi Gas, *Phys. Rev. Lett.* **122**, 203402 (2019).
- [47] B. Nagler, K. Jägering, A. Sheikhan, S. Barbosa, J. Koch, S. Eggert, I. Schneider, and A. Widera, Dipole oscillations of fermionic quantum gases along the BEC-BCS crossover in disordered potentials, *Phys. Rev. A* **101**, 053633 (2020).
- [48] J. Koch, K. Menon, E. Cuestas, S. Barbosa, E. Lutz, T. Fogarty, T. Busch, and A. Widera, A quantum engine in the BEC-BCS crossover, *Nature* **621**, 723 (2023).
- [49] M. Jäger and J. H. Denschlag, Methods for studying Tan's contact in the BCS-BEC crossover, *Phys. Rev. A* **109**, 063330 (2024).
- [50] D. J. Young, E. Y. Song, A. Chu, D. Barberena, Z. Niu, V. M. Schäfer, R. J. Lewis-Swan, A. M. Rey, and J. K. Thompson, Time-Resolved Spectral Gap Spectroscopy in a Quantum Simulator of Fermionic Superfluidity inside an Optical Cavity, *Phys. Rev. Lett.* **134**, 183404 (2025).
- [51] Z. Su, T.-H. Shou, H. Yang, J. Cao, B.-Y. Wang, T. Xie, J. Rui, B. Zhao, and J.-W. Pan, Broad Feshbach Resonance with a Large Background Scattering Length in a Fermionic Atom-Molecule Mixture, *Phys. Rev. Lett.* **135**, 213401 (2025).
- [52] R. Combescot, M. Y. Kagan, and S. Stringari, Collective mode of homogeneous superfluid Fermi gases in the BEC-BCS crossover, *Phys. Rev. A* **74**, 042717 (2006).
- [53] H. Kurkjian, S. N. Klimin, J. Tempere, and Y. Castin, Pair-Breaking Collective Branch in BCS Superconductors and Superfluid Fermi Gases, *Phys. Rev. Lett.* **122**, 093403 (2019).
- [54] T. Enss, Bulk Viscosity and Contact Correlations in Attractive Fermi Gases, *Phys. Rev. Lett.* **123**, 205301 (2019).
- [55] S. N. Klimin, J. Tempere, and H. Kurkjian, Phononic collective excitations in superfluid Fermi gases at nonzero temperatures, *Phys. Rev. A* **100**, 063634 (2019).
- [56] S. Van Loon, J. Tempere, and H. Kurkjian, Beyond Mean-Field Corrections to the Quasiparticle Spectrum of Superfluid Fermi Gases, *Phys. Rev. Lett.* **124**, 073404 (2020).
- [57] S. N. Klimin, J. Tempere, and H. Kurkjian, Collective excitations of superfluid Fermi gases near the transition temperature, *Phys. Rev. A* **103**, 043336 (2021).
- [58] S. Van Loon and C. A. R. Sá de Melo, Effects of Quantum Fluctuations on the Low-Energy Collective Modes of Two-Dimensional Superfluid Fermi Gases from the BCS to the Bose Limit, *Phys. Rev. Lett.* **131**, 113001 (2023).
- [59] J. Verstraten, K. Dai, M. Dixmerias, B. Peaudecerf, T. de Jongh, and T. Yefsah, In Situ Imaging of a Single-Atom Wave Packet in Continuous Space, *Phys. Rev. Lett.* **134**, 083403 (2025).
- [60] J. Xiang, E. Cruz-Colón, C. C. Chua, W. R. Milner, J. de Hond, J. F. Fricke, and W. Ketterle, In Situ Imaging of the Thermal de Broglie Wavelength in an Ultracold Bose Gas, *Phys. Rev. Lett.* **134**, 183401 (2025).
- [61] R. Yao, S. Chi, M. Wang, R. J. Fletcher, and M. Zwierlein, Measuring Pair Correlations in Bose and Fermi Gases via Atom-Resolved Microscopy, *Phys. Rev. Lett.* **134**, 183402 (2025).
- [62] T. de Jongh, J. Verstraten, M. Dixmerias, C. Daix, B. Peaudecerf, and T. Yefsah, Quantum Gas Microscopy of Fermions in the Continuum, *Phys. Rev. Lett.* **134**, 183403 (2025).
- [63] C. Daix, M. Dixmerias, Y.-Y. He, J. Verstraten, T. de Jongh, B. Peaudecerf, S. Zhang, and T. Yefsah, Observing Spatial Charge and Spin Correlations in a Strongly-Interacting Fermi Gas (2025), arXiv:2504.01885.
- [64] C. Daix, P. M. Tam, M. Dixmerias, J. Verstraten, T. de Jongh, B. Peaudecerf, C. L. Kane, and T. Yefsah, Probing the Fermi Sea Topology in a Quantum Gas (2025), arXiv:2511.23353 [cond-mat.quant-gas].
- [65] W. S. Bakr, J. I. Gillen, A. Peng, S. Fölling, and M. Greiner, A quantum gas microscope for detecting single atoms in a Hubbard-regime optical lattice, *Nature* **462**, 74 (2009).
- [66] J. G. Danzl, M. J. Mark, E. Haller, M. Gustavsson, R. Hart, J. Aldegunde, J. M. Hutson, and H.-C. Nägerl, An ultracold high-density sample of rovibronic ground-state molecules in an optical lattice, *Nat. Phys.* **6**, 265 (2010).
- [67] L. W. Cheuk, M. A. Nichols, M. Okan, T. Gersdorf, V. V. Ramasesh, W. S. Bakr, T. Lompe, and M. W. Zwierlein, Quantum-Gas Microscope for Fermionic Atoms, *Phys. Rev. Lett.* **114**, 193001 (2015).
- [68] L. W. Cheuk, M. A. Nichols, K. R. Lawrence, M. Okan, H. Zhang, E. Khatami, N. Trivedi, T. Paiva, M. Rigol, and M. W. Zwierlein, Observation of spatial charge and spin correlations in the 2D Fermi-Hubbard model, *Science* **353**, 1260 (2016).
- [69] S. Hollerith, J. Zeiher, J. Rui, A. Rubio-Abadal, V. Walther, T. Pohl, D. M. Stamper-Kurn, I. Bloch, and C. Gross, Quantum gas microscopy of Rydberg macrodimers, *Science* **364**, 664 (2019).
- [70] C. Gross and W. S. Bakr, Quantum gas microscopy for single atom and spin detection, *Nat. Phys.* **17**, 1316 (2021).
- [71] A. M. Kaufman and K.-K. Ni, Quantum science with optical tweezer arrays of ultracold atoms and molecules, *Nat. Phys.* **17**, 1324 (2021).
- [72] S. Kangjun and C. A. R. Sá de Melo, Compressibility and spin susceptibility in the evolution from BCS to BEC superfluids (2011), arXiv:1105.4365.
- [73] R. L. Stratonovich, On a Method of Calculating Quantum Distribution Functions, *Sov. Phys. Dokl.* **2**, 416 (1957).
- [74] J. Hubbard, Calculation of Partition Functions, *Phys. Rev. Lett.* **3**, 77 (1959).
- [75] E. E. Salpeter and H. A. Bethe, A Relativistic Equation for Bound-State Problems, *Phys. Rev.* **84**, 1232 (1951).
- [76] S. S. Botelho and C. A. R. Sá de Melo, Vortex-Antivortex Lattice in Ultracold Fermionic Gases, *Phys. Rev. Lett.* **96**, 040404 (2006).
- [77] Y. Castin, Pair distribution functions of a superfluid spin-1/2 Fermi gas with contact interactions in the linearized time-dependent BCS theory (2026), arXiv:2601.01985 [cond-mat.quant-gas].

## END MATTER

*Appendix A: Response functions* Performing a Fourier transformation on the fermions

$$c_s(\mathbf{k}, ik_n) = \int_0^\beta \frac{d\tau}{\beta} \int \frac{d^D x}{\sqrt{L^D}} \psi_s(\mathbf{x}, \tau) e^{-i\mathbf{k}\cdot\mathbf{x} + ik_n \tau}, \quad (\text{A1})$$

and integrating them through a standard procedure [40], leads to the dimensionless effective action

$$S_{\text{eff}}[j_s] = \beta L^D \sum_q \frac{|\Delta_q|^2}{g} - \sum_{kk'} \ln \text{Det} [\beta \mathbf{G}^{-1}]. \quad (\text{A2})$$

Here, the label  $q = (\mathbf{q}, iq_\ell)$  represents momentum  $\mathbf{q}$  bosonic Matsubara frequency  $q_\ell$ , and Det as determinant over all degrees of freedom, Using the momentum space relation  $\Delta_q = \int_0^\beta \frac{d\tau}{\beta} \int \frac{d^D x}{L^D} \Delta(x) e^{-i\mathbf{q}\cdot\mathbf{x} + iq_\ell \tau}$ , we obtain

$$\mathbf{G}^{-1}(k, k') = \begin{pmatrix} \alpha_\uparrow(k, k') + j_{\uparrow, k-k'} & \Delta_{k-k'} \\ \Delta_{k'-k} & \alpha_\downarrow(k, k') - j_{\downarrow, k-k'} \end{pmatrix}. \quad (\text{A3})$$

with diagonal terms  $\alpha_\uparrow(k, k') = (ik_n - \xi_{\uparrow, \mathbf{k}}) \delta_{k, k'}$  and  $\alpha_\downarrow(k, k') = (ik_n + \xi_{\downarrow, \mathbf{k}}) \delta_{k, k'}$  involve the kinetic energies  $\xi_{s, \mathbf{k}} = \mathbf{k}^2/2m_s - \mu_s$  with respect to the chemical potentials  $\mu_s$  using  $k = (\mathbf{k}, ik_n)$  with momentum  $\mathbf{k}$  and fermionic Matsubara frequency  $k_n$ . The term  $j_{s, q}$  is related to  $j_s(x)$  via the transformation  $j_{s, \mathbf{k}, ik_n} = \int_0^\beta \frac{d\tau}{\beta} \int \frac{d^D x}{L^D} j_s(\mathbf{x}, \tau) e^{-i\mathbf{k}\cdot\mathbf{x} + ik_n \tau}$ .

Since our goal is to compute the locally gauge-invariant *spin*-resolved density-density correlation functions, it is essential to include the gauge freedom of the pair field. We decompose  $\Delta_q = \Delta_0 \delta_{q, 0} + \lambda_q + i\theta_q$ , where  $\Delta_0$  is the uniform order parameter and  $\lambda_q$  and  $\theta_q$  are real fields necessary to guarantee the local gauge invariance of the full *spin*-dependent density-density correlations.

We expand  $S_{\text{eff}}[j_s]$  to quadratic order in  $\lambda_q$  and  $\theta_q$ , followed by an expansion to Gaussian order in  $j_{s, q}$ . This procedure gives three contributions

$$S_{\text{eff}}[j_s] = \mathcal{S}_0 + \mathcal{S}_1[j_s] + \mathcal{S}_2[j_s, \lambda, \theta] + \mathcal{O}(j_s^3, \lambda^3, \theta^3). \quad (\text{A4})$$

The leading order term of the effective action is

$$\mathcal{S}_0 = \beta L^D \frac{|\Delta_0|^2}{g} - \sum_k \ln \det [\beta \mathbf{G}_0^{-1}(k)]. \quad (\text{A5})$$

where the saddle-point inverse Green's function is

$$\mathbf{G}_0^{-1}(k) = \begin{pmatrix} \alpha_\uparrow(k, k) & \Delta_0 \\ \Delta_0 & \alpha_\downarrow(k, k) \end{pmatrix}. \quad (\text{A6})$$

Extremizing  $\mathcal{S}_0$ , that is,  $\partial \mathcal{S}_0 / \partial \bar{\Delta}_0 = 0$ , leads to

$$\Delta_0 = \frac{g}{\beta L^D} \sum_k \text{tr} \left\{ \mathbf{G}_0(k) \frac{\partial \mathbf{G}_0^{-1}(k)}{\partial \bar{\Delta}_0} \right\}. \quad (\text{A7})$$

The first order correction is

$$\mathcal{S}_1[j_s] = - \sum_{k, s} G_{0, ss}(k) j_{s, 0}, \quad (\text{A8})$$

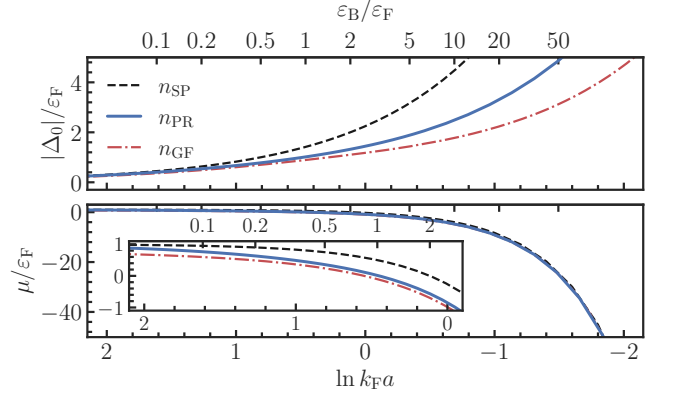


FIG. 4. Self-consistent results for  $|\Delta_0|/\varepsilon_F$  (top panel) and  $\mu/\varepsilon_F$  (bottom panel) versus  $\ln k_F a$  (lower  $x$ -axis) or binding energy  $\varepsilon_B/\varepsilon_F$  (upper  $x$ -axis). The dashed black line shows the saddle-point (SP), the dash-dotted red line describes the Gaussian fluctuations (GF), while the solid blue line represents the Pauli-respecting (PR) equation of state (EoS).

where  $G_{0, ss}$  is a diagonal matrix element of  $\mathbf{G}_0$ . The linear terms in  $\lambda$  and  $\theta$  vanish due to the saddle-point condition in Eq. (A7). The second term is

$$\mathcal{S}_2[j_s, \lambda, \theta] = \frac{\beta}{2} \sum_q \phi_{-q}^T \mathbf{\Pi}(q) \phi_q, \quad (\text{A9})$$

where the fields  $\phi_{-q}^T = (j_{-q}^T \ \eta_{-q}^T)$  have dimensions of energy and include the real and imaginary fluctuations of the pair field  $\eta_{-q}^T = (\lambda_{-q} \ \theta_{-q})$ ; while the source currents  $j_{-q}^T = (j_{\uparrow, -q} \ j_{\downarrow, -q})$  play the role of a non-uniform fluctuation in the chemical potentials  $\mu_\uparrow$  and  $\mu_\downarrow$ . The elements of  $\mathbf{\Pi}$ , having dimensions of inverse energy, are

$$\Pi_{ab}(q) = v_{ab} + \frac{(-1)^{\zeta_{ab}}}{\beta} \sum_k \text{tr} \{ \mathbf{G}_0(k) \gamma_a \mathbf{G}_0(k+q) \gamma_b \}, \quad (\text{A10})$$

where  $v_{ab} = 2\delta_{ab}\zeta_{ab}/(L^D g)$ ,  $\zeta_{ab} = \delta_{ax} + \delta_{ay}$ , and  $\{a, b\} \in \{\uparrow, \downarrow, x, y\}$ . The  $\gamma_a$  are  $2 \times 2$  matrices defined as  $\gamma_\uparrow = (\mathbf{I} + \sigma_z)/2$ ,  $\gamma_\downarrow = (\mathbf{I} - \sigma_z)/2$ ,  $\gamma_x = \sigma_x$ ,  $\gamma_y = \sigma_y$ , where  $\mathbf{I}$  is the identity, and  $\sigma_x$ ,  $\sigma_y$  and  $\sigma_z$  are Pauli matrices.

The notation above simplifies the description of  $\mathbf{\Pi}$ , but hides its physical meaning, thus we write

$$\mathbf{\Pi}(q) = \begin{pmatrix} \Pi_{\uparrow\uparrow}(q) & \Pi_{\uparrow\downarrow}(q) & \Pi_{\uparrow x}(q) & \Pi_{\uparrow y}(q) \\ \Pi_{\downarrow\uparrow}(q) & \Pi_{\downarrow\downarrow}(q) & \Pi_{\downarrow x}(q) & \Pi_{\downarrow y}(q) \\ \Pi_{x\uparrow}(q) & \Pi_{x\downarrow}(q) & \Pi_{xx}(q) & \Pi_{xy}(q) \\ \Pi_{y\uparrow}(q) & \Pi_{y\downarrow}(q) & \Pi_{yx}(q) & \Pi_{yy}(q) \end{pmatrix} \quad (\text{A11})$$

$$= \begin{pmatrix} \tilde{\chi}_0(q) & \Lambda^T(q) \\ \Lambda(q) & \Gamma(q) \end{pmatrix} \quad (\text{A12})$$

in a block-diagonal form. The matrix elements  $\tilde{\chi}_0(q)$  are simply source-source (jj) correlation functions, that is, the symbols  $\{\uparrow, \downarrow\}$  represent  $\{j_\uparrow, j_\downarrow\}$ , respectively. The matrix  $\Lambda(q)$  describes the coupling between the source terms  $\{j_\uparrow, j_\downarrow\} \leftrightarrow \{\uparrow, \downarrow\}$  and the pair fluctuations

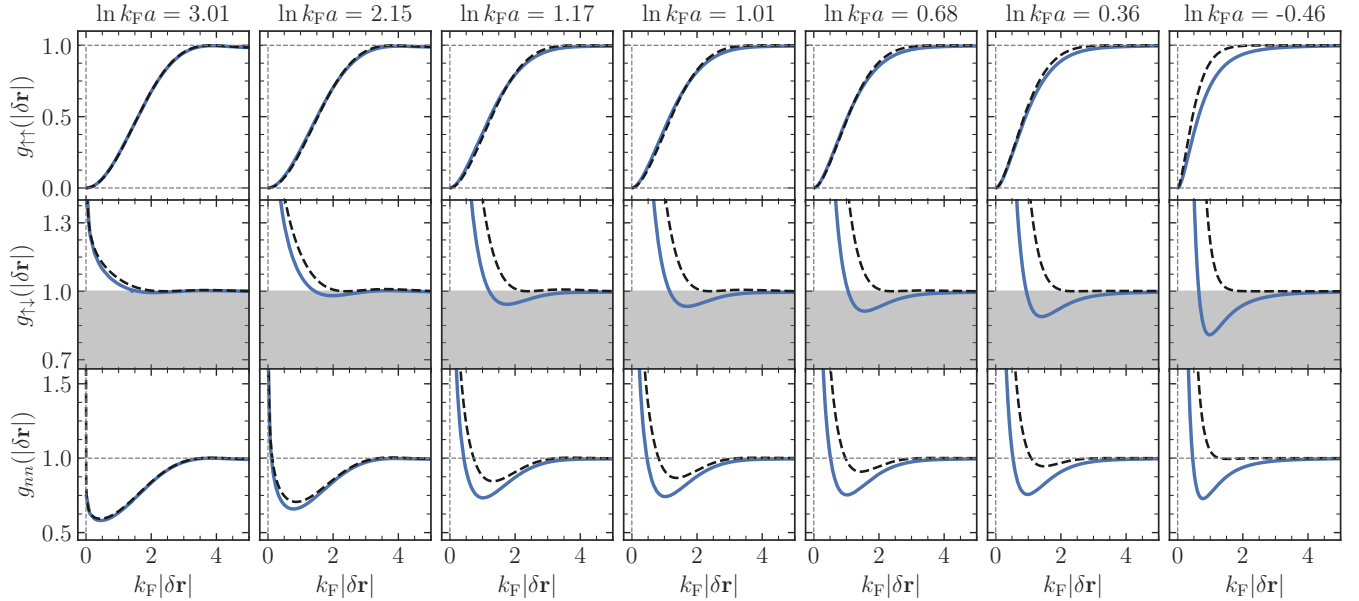


FIG. 5. Numerical results for  $g_{\uparrow\uparrow}(\delta\mathbf{r})$  (top panel),  $g_{\uparrow\downarrow}(\delta\mathbf{r})$  (middle panel) and  $g_{nn}(\delta\mathbf{r})$  (bottom panel) versus  $k_F|\delta\mathbf{r}|$ . The dashed black (solid blue) lines illustrate case I (IV) in table I. We use  $\ln k_F a$  from 3.01 (BCS regime) to  $-0.46$  (BEC region).

$\{\lambda, \theta\} \leftrightarrow \{x, y\}$ . The block matrix  $\mathbf{\Gamma}(q)$  represents the pair fluctuations only  $\{\lambda, \theta\} \leftrightarrow \{x, y\}$ . Integrating out the fluctuation fields  $\boldsymbol{\eta}_q$  leads to

$$\mathcal{S}_{\text{eff}}[j_s] = \mathcal{S}_{\text{GF}} + \mathcal{S}_1[j_s] + \mathcal{S}_2[j_s], \quad (\text{A13})$$

where the Gaussian fluctuation action is

$$\mathcal{S}_{\text{GF}} = \mathcal{S}_0 + \sum_q \ln \det [\beta \mathbf{\Gamma}(q)]. \quad (\text{A14})$$

Here  $\mathcal{S}_1$  is defined in Eq. (A8) and  $\mathcal{S}_2[j_s]$  is given Eq. (18) of the main text.

From  $\mathcal{S}_2[j_s]$ , we can read off  $\tilde{\chi}(q) = \tilde{\chi}_0(q) + \tilde{\chi}_{\text{irr}}(q)$ , displayed in Eq. (19) of the main text. The first term  $\tilde{\chi}_0(q)$  contains the connected two-particle-reducible contributions and a constant term from the singular part of  $\chi_{ss'}(\delta\mathbf{r})$ . The second term  $\tilde{\chi}_{\text{irr}}(q) = -\mathbf{\Lambda}^T(-q)\mathbf{\Gamma}^{-1}(q)\mathbf{\Lambda}(q)$  represents the two-particle irreducible contribution describing collective excitations, many-body scattering states and vertex corrections. For instance, the integer zeros of  $\mathbf{\Gamma}(q)$  represent the collective excitations due to pair fluctuations. When relating the matrix elements  $\tilde{\chi}_{ss'}(q)$  to the dynamical structure factor tensor  $S_{ss'}(q)$ , the contribution from  $\chi_{\text{irr},ss'}(q)$  is essential to fulfill the compressibility sum rule and the f-sum rule [20, 72].

The action  $\mathcal{S}_{\text{GF}}$  in Eq. (A14) gives the GF EoS

$$n_s = \frac{1}{L^D \beta} \sum_k G_{0,ss}(k) - \frac{1}{2L^D \beta} \sum_q \frac{\partial}{\partial \mu_s} \ln \det [\beta \mathbf{\Gamma}(q)], \quad (\text{A15})$$

where the first term comes from  $\mathcal{S}_0$  and represents the SP EoS, whereas the second is due to pair fluctuations.

*Crossover in 2D:* Two-dimensional ( $D = 2$ ) systems exhibit a two-body bound state with binding energy  $\varepsilon_B$  for arbitrarily small contact interactions. In contrast, there is a threshold for the emergence to two-body bound states for three dimensions ( $D = 3$ ). Furthermore, in 3D, the inclusion of longitudinal fluctuations in  $\lambda, \theta$  are sufficient to describe the BCS-BEC crossover at finite temperatures. However, in 2D, we must also include transverse fluctuations (vortices and antivortices) due to Berezinskii-Kosterlitz-Thouless (BKT) mechanism. Thus, we investigate the experimentally relevant example of a 2D Fermi system with balanced masses ( $m_\uparrow = m_\downarrow = m$ ) and populations ( $n_\uparrow = n_\downarrow = n/2$ ) at  $T = 0$ .

In Fig. 4, using the Fermi energy  $\varepsilon_F$ , we show self-consistent solutions of  $|\Delta_0|/\varepsilon_F$  and  $\mu/\varepsilon_F$  for: saddle-point (SP) (dashed-black line), saddle-point plus Gaussian fluctuations (GF) (dashed-dotted red line) and Pauli-respecting (PR) (solid blue). The results for  $|\Delta_0|/\varepsilon_F$  ( $\mu/\varepsilon_F$ ) are illustrated in the top (bottom) panel versus  $\ln k_F a$  ( $\varepsilon_B/\varepsilon_F$ ) depicted as lower (upper)  $x$ -axis. The values of  $|\Delta_0|/\varepsilon_F$  and  $\mu/\varepsilon_F$  for the PR equation of state (EoS) always lie between SP and GF results.

In Fig. 5, we present an extension of the data found in Fig. 2 of the main text. The interaction parameters range now from  $\ln k_F a = 3.01$  (deeper into the BCS region) to  $\ln k_F a = -0.46$  (further into the BEC regime). The plots in Fig. 5 further support the findings in the main text.